Physica C 209 (1993) 477–485
North-Holland

PHYSICA C

Fabrication of Nb/Al,AlO_x/Al/Nb Josephson tunnel junctions using reactive ion etching in SF_6

D.J. Adelerhof [a], M.E. Bijlsma [a], P.B.M. Fransen [a], T. Weiman [b], J. Flokstra [a] and H. Rogalla [a]

[a] *Department of Applied Physics, Low Temperature Group, University of Twente, PO Box 217, 7500 AE Enschede, Netherlands*

[b] *Physikalische Technische Bundesanstalt, Bundesallee 100, D-33 Braunschweig, Germany*

Received 19 February 1993

High quality Nb/Al,AlO_x/Al/Nb Josephson tunnel junctions have been made with the help of a fabrication process based on reactive ion etching of Nb in SF_6. The V_m value of these junctions is typically 60–70 mV at 4.2 K. At 1.6 K, a V_m of 4.1 V has been measured, which is the highest value that has ever been reported for this type of junction. The area of the junctions ranges from 1 to 25 μm^2. By burying the Nb/Al,AlO_x/Al/Nb trilayer in the substrate, a planarized junction configuration has been obtained. Reactive ion etching of Nb in SF_6 plasmas has been studied in detail. Anisotropic etch profiles can be obtained because of the formation of a resistant layer during etching, which prevents etching of Nb under the photoresist. The etching process has been monitored with a spectrometer. The fluorine emission at 703.7 nm is shown to be suitable for end point detection.

1. Introduction

Since the introduction of Nb/Al,AlO_x/Nb Josephson tunnel junctions [1], the number of groups utilizing these junctions has vastly increased, because they offer long term stability and are stable against thermal cycling. Their critical temperature is high enough to be operated at liquid helium temperature and the quality of the junctions can be very high [2–6].

In applications like DC-SQUIDs and X-ray detectors based on Josephson tunnel junctions the performance of the device is directly related to the junction quality. In DC-SQUIDs it is well known that zero voltage current fluctuations in the junctions cause excess $1/f$ noise in the spectral flux noise density of the SQUID. This current induced excess noise can be reduced by using an appropriate read out scheme [7,8], which, however, increases the complexity of the read out electronics considerably. The critical current fluctuations are related to the quality of the insulating barrier. Due to inhomogeneities in the barrier, like for instance localized states in which electrons can be trapped and released [9,10], the junction resistance and consequently the critical current fluctuates. It is expected that these fluctuations will be smaller in junctions of higher quality. An important parameter for X-ray detectors is the dynamic subgap resistance [11]. Leakage currents should be as low as possible and the aim is to reach the temperature dependent BCS quasiparticle current value at an operation temperature of about 1 K.

In recent publications [3,12] Nb/Al,AlO_x(/Al)Nb junctions made at the University of Twente have been discussed. These junctions were fabricated by selective niobium anodization (SNAP). The minimum junction size was 25 μm^2. It was found that the deposition of an extra Al layer on top of the AlO_x barrier, prior to deposition of the Nb counter electrode, significantly increased the reproducibility of the fabrication of high quality junctions. It was also found that the junction quality parameter V_m decreased with decreasing junction area. This effect was related to barrier inhomogeneities introduced during the anodization process.

A new fabrication process has been initiated for the production of Nb/Al,AlO_x/Al/Nb SNINS Josephson tunnel junctions. The fabrication process has systematically been optimized in order to obtain planarized small area junctions of very high quality. Planarization relieves the deposition conditions for insulating layers and crossing lines and facilitates the

deposition of resistive elements. Since SNAP appears to be unsuited for the fabrication of small area, high quality junctions, the anodization process has been replaced by a selective niobium etching process (SNEP).

Selective niobium etching can be done by reactive ion etching (RIE) in fluorine containing plasmas of for instance CF_4 or SF_6 [13–15]. Because in these plasmas the etch rate of Nb is much larger than the etch rate of Al, the Al layer can be used as an etch stop. We have studied RIE of niobium in SF_6. The etch rates of Nb and Al were measured under different plasma conditions. The etching process is monitored by a spectrometer in order to detect the end point of the RIE process. The results are discussed in section 2.

In section 3 the junction fabrication procedure is described. The area of the fabricated junctions varies from 1 to 25 μm^2. Part of these junctions have different base electrode dimensions in order to verify whether the sputtered Nb films are free of stress.

The junction I–V characteristics are discussed in section 4. Subgap currents have been measured at 4.2 and 1.6 K in order to study the quality of the insulating barrier of the junctions. The characteristics are compared to the BCS theory.

2. Reactive ion etching of Nb with SF_6

Reactive ion etching is done in a turbo pumped parallel plate reactor with stainless steel electrodes. Samples are glued with vacuum grease to a stainless steel substrate holder with a diameter of 10 cm and a thickness of 3 mm. The substrate holder can be clamped onto the cathode through a load-lock system. The diameter of the water cooled cathode is 15 cm. The grounded anode has a diameter of 20 cm and is positioned at 4.5 cm from the cathode.

The background pressure is measured by a cold cathode gauge, the pressure during sputtering is measured by a Pirani gauge, calibrated to air. The pressure reading of the Pirani is multiplied by conversion factors of 1.6 and 0.3 to calculate the actual Ar and SF_6 pressure, respectively. The background pressure is about 2×10^{-5} Pa. The purity of the SF_6 is 99.99%.

The progress of the RIE process is monitored with a spectrometer. The monochromator can be adjusted from 200 to 800 nm, with a resolution of 2 nm. The plasma is monitored through a quartz window in the etching chamber. The transmission of the quartz window is more than 90% at wavelengths larger than 280 nm. The transmission decreases to about 50% from 280 down to 200 nm.

The optical spectra of two plasmas are shown in fig. 1. One of the spectra is of an SF_6 plasma without sample, the other is the spectrum during etching of a Nb foil of 5×5 cm^2 in an SF_6 plasma, taken 5 min after ignition of the plasma. The plasma parameters are: SF_6 pressure 1.5 Pa, flow rate 5 sccm, power density 0.13 W/cm^2 and DC self-bias voltage -100 V. The emission at wavelengths larger than 620 nm can be assigned to fluorine radicals and F^+ ions [16,17]. The $2P^0\rightarrow2P$ transition at 703.7 nm shows the strongest emission intensity of fluorine radicals. The emissions at 316, 337, and 358 nm, clearly visible in the SF_6 plasma without Nb, are possibly due to small N_2 contaminations in the reactor [18].

The most pronounced differences in the two spectra can be observed below 600 nm. The change in colour of the plasma as soon as the Nb etching starts can also be observed by the eye. In principle, one of the emissions in the range from 290 to 600 nm can be used to monitor the RIE process. Since we do not know which molecule or atom this emission can be

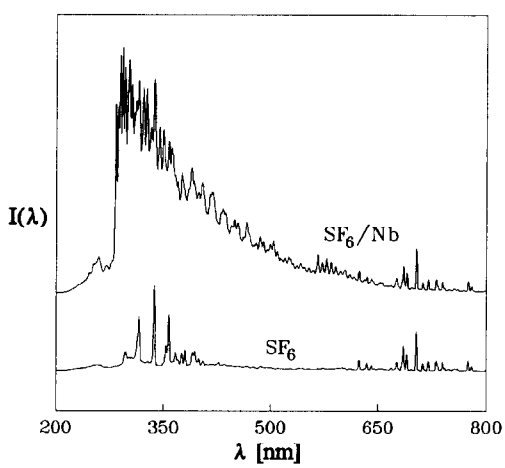

Fig. 1. Emission spectra of two SF_6 plasmas: one with a Nb foil of 25 cm^2 stuck to the substrate holder (upper curve) and one without a Nb sample. The origin of the upper curve is shifted, the intensity scales are identical.

assigned to, the suitability of the fluorine emission at 703.7 nm for monitoring the etching process has been investigated.

In fig. 2 the emission at 703.7 nm is shown as a function of time during etching of 8 Nb samples. The samples consisted of 1×1 cm^2 of oxidized Si with 6 nm Al and 300 nm Nb. The etching time of the samples was different. The amounts of Nb and Al etched away were measured for all samples and are depicted in fig. 2 as well. From the figure it is clear that an initiation time of about 30 s is present during which the Nb etch rate is very low. After this initiation time the Nb etch rate is constant at a level of about 60 nm/min. The etch rate strongly decreases when the Al layer is reached. The emission intensity at 703.7 nm increases as long as Nb is being etched and decreases when no Nb is left on the sample and the Al layer is reached. Figure 2 clearly shows that the fluorine emission at 703.7 nm can be used to detect the end point of the Nb etch process.

The etching experiments of which the results are presented in fig. 2 were obtained after cleaning the electrodes and substrate holder. In the cleaning procedure an SF_6/O_2 plasma is used to remove remaining NbF_x etch products. Especially Nb sub-fluorides (NbF_x, $x \leq 4$) will be present in the reactor since they are solid at room temperature [19]. NbF_5 is also solid but it has a vapour pressure of 0.5 Pa at 20°C and 10 Pa at 40°C and will be pumped away during etching. The SF_6/O_2 plasma is followed by a pure O_2 plasma to remove sulphur and a subsequent Ar plasma for physical cleaning of the electrodes. The complete cleaning procedure takes about 40 min, but is essential for obtaining reproducible results. Without cleaning, the etch rate may increase by a factor of two, depending on the history of the reactor.

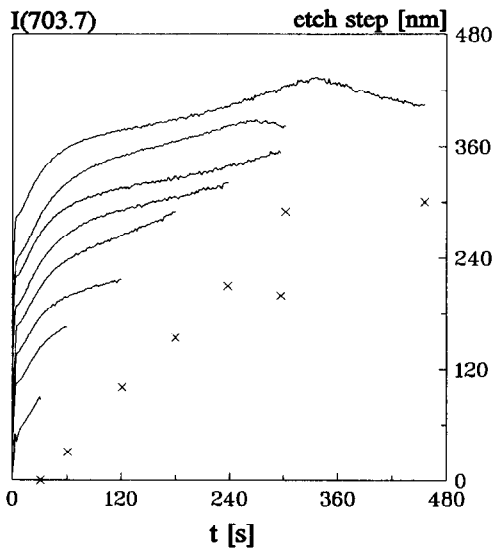

Fig. 2. RIE in SF_6 of 8 samples consisting of 1 cm^2 of oxidized Si with 6 nm Al and 300 nm Nb. The solid lines are the intensities of the fluorine emission at 703.7 nm (left axis) as a function of time. The origins of the 8 different curves are shifted vertically for clarity. The plasma was turned on at $t = 0$ and turned off after 30, 60, 120, 180, 240, 295, 304, or 460 s. The thickness of the removed layer after the RIE is depicted by crosses (right axis).

The effect of the Nb sample area on the fluorine emission during RIE has been investigated as well. Five samples consisting of 300 nm Nb on top of 6 nm Al with areas of 1, 2, 3, 5 and 10 cm^2 were etched while the emission intensity at 703.7 nm was measured. Up to a sample area of 3 cm^2 the fluorine emission revealed the RIE end point quite clearly. With larger sample areas the large amount of NbF_x etch products affected the fluorine emission significantly and the exact end point was more difficult to determine. We observed that the Nb etch rate increased by 30% when the sample area was increased from 1 to 3 cm^2. At a further increase of the sample area to 10 cm^2 the etch rate decreased again. This effect needs to be studied further before any conclusions can be drawn.

The suitability of the Al layer as an etch stop depends on the DC self-bias voltage on the cathode during the RIE process. This is shown in fig. 3. Three samples of 1 cm^2 consisting of two layers of 150 nm Nb separated by 6 nm of Al deposited on oxidized Si have been etched in an SF_6 plasma at 1.5 Pa. The RF powers used were 20, 50 and 85 W, resulting in DC self-bias voltages of -100, -200, and -300 V, respectively. In this experiment the reactor was not pre-cleaned.

The Nb/Al/Nb trilayers of the samples that were etched for 20 min at -300 and -200 V were completely etched away. At -100 V, only the top Nb layer is etched away. So, at this self-bias voltage the time needed to etch away an Al layer of only 6 nm is at least 18 min. At self-bias voltages of -200 V or higher, 6 nm of Al is no longer a good etch stop for RIE of Nb films in SF_6.

In the junction fabrication process, which will be

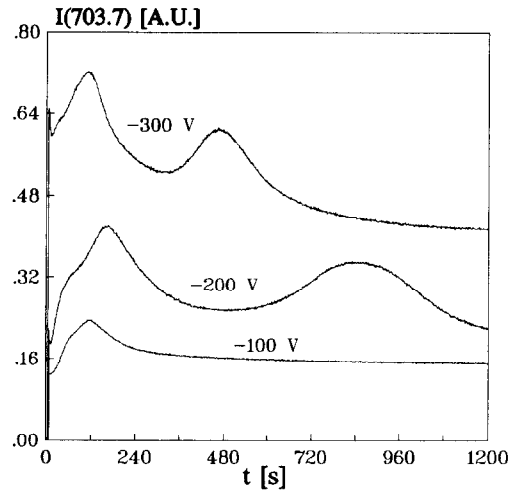

Fig. 3. Fluorine emission intensity vs. time during etching of three identical samples, consisting of a trilayer of 150 nm Nb, 6 nm Al, and 150 nm Nb on top of 1 cm^2 of oxidized Si. The origins of the three curves coincide. The samples were etched at three different self-bias voltages: -100, -200, and -300 V.

Fig. 4. SEM picture of a sample of 600 nm Nb on top of 6 nm of Al etched in an SF_6 plasma identical to the SF_6 plasma that was used for the measurements shown in fig. 2. The plasma was turned off 3 min after the exposed Nb was etched away. The rough surface of the etched parts of the sample is probably due to reaction products ((——) $\cong 1$ μm).

described in section 3, etching of Nb under the photo resist has to be avoided. In fig. 4 a SEM picture is shown of an etched Nb film with a photo resist pattern on top of it. The Nb film has been etched in an SF_6 plasma at a self-bias voltage of -100 V. The etching was stopped by a thin Al layer. The plasma was turned off three minutes after the Al layer was reached. It is clear that no undercetching has occurred. In fig. 5 a SEM picture of a Nb film that has been etched in an SF_6/O_2 (5:1) mixture at a self-bias voltage of -100 V is shown. This time, strong etching under the photo resist did occur. The Nb is almost isotropically etched.

Apparently, during Nb etching in a pure SF_6 plasma an etch resistant layer is formed on the sides of the part of the Nb film that is covered by photo resist. By addition of a small amount of O_2 to the SF_6 plasma the resistant layer is not formed. The protective layer probably contains carbon, which can be supplied by the photo resist.

A third experiment has been performed which nicely demonstrates the presence of an etch resistant layer. From a Nb sample identical to the one shown in fig. 5, the photo resist pattern was dissolved in acetone after the RIE in pure SF_6. Then the sample was remounted in the reactor and was etched for the second time in a pure SF_6 plasma with a self-bias voltage of -100 V. Again, the plasma was turned off 3 min after the Nb film was gone. The SEM picture of the resulting structure is shown in fig. 6. The sidewalls of the part of the Nb film that was covered by the resist during the first RIE are still present. So, during etching of Nb in a pure SF_6 plasma, indeed

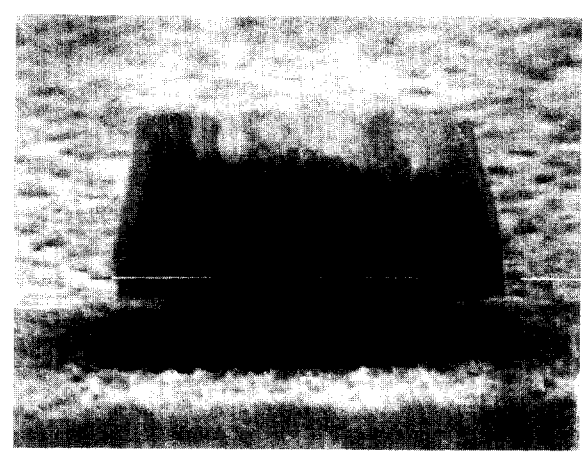

Fig. 5. SEM picture of a sample of 600 nm Nb on top of 6 nm of Al etched in an SF_6/O_2 plasma of 5 sccm of SF_6 and 1 sccm of O_2, at a self-bias voltage of -100 V. The plasma was turned off 3 min after the Al layer was reached ((——) $\cong 1$ μm).

Fig. 6. SEM picture of the etch resistant layer formed during RIE in pure SF_6 on the sides of the part of the Nb film that is covered by photo resist ((——) ≅ 1 μm).

an etch resistant layer with a thickness of about 0.1 μm is formed on the sides of the Nb film.

3. The junction fabrication process

On a 2 inch Si wafer, junctions of 1×1, 2×2, 3×3, and 5×5 μm^2 have been made. To check whether the Nb films are free of stress, the base electrode dimensions of junctions of 2×2 and 3×3 μm^2 have been varied [20]: 10×10, 15×15, 30×30, 50×50, and 100×100 μm^2. The junctions are located in the center of the base electrodes. Chromium lithography masks with a minimum feature size of 1 μm were used.

The fabrication process of the junctions is shown schematically in fig. 7. The fabrication starts with the spinning of 1.5 μm of photo resist (AZ 1518) onto a thermally oxidized Si wafer. The resist is structured and post-baked.

After lithography, 400 nm of SiO_2 is etched away by wet chemical etching in a solution of 6.5 wt.% HF, 34.8 wt.% NH_4F and 58.7 wt.% H_2O (fig. 7(a)). The temperature is kept constant at 30°C. The SiO_2 etch rate of about 160 nm/min can be reproduced within 5%. The etch rate of the photo resist in the HF solution is very low, provided that the resist has been baked at 120°C for 45 min. Since the SiO_2 is etched isotropically, strong under-etching of the SiO_2 occurs. This underetch, or vice versa the photo resist overhang, can prevent the formation of so-called "ears" after lift-off of a subsequently sputter deposited Nb/Al trilayer.

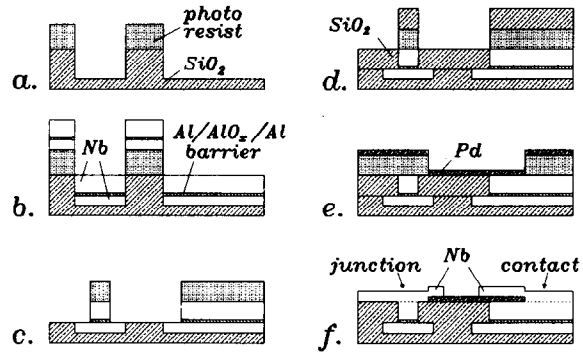

Fig. 7. Schematic overview of the fabrication process of planarized, small area Nb/Al,AlO_x/Al/Nb tunnel junctions made by SNEP. See text for additional information.

Nb and Al films are deposited in a turbo pumped vacuum system by DC magnetron sputtering (fig. 7(b)). The effective target area is 63 cm^2. The background pressure is typically 2×10^{-5} Pa, mainly due to water vapor. The background pressure is reduced to below 6×10^{-6} Pa by Nb getter sputtering. The residual gases are monitored by a mass spectrometer. The total pressure is measured by an ion gauge. During sputtering, the pressure is measured by a capacitance manometer.

In Nb/AlO_x/Nb junctions defined by SNEP, stress in the Nb electrodes may decrease the junction quality [20]. With the help of flexible glass substrates the stress in Nb films deposited under different sputtering conditions has been investigated. The stress was calculated from the deflection of the substrates [21]. Since it was expected that the stress would change with changing cathode voltage [22,23], the Ar pressure during sputtering was kept constant at 2.0 Pa and the sputter voltage was varied from 240 V to 320 V. Consequently, the power density and the deposition rate varied from 0.5 to 6.1 W/cm^2 and from 9 to 115 nm/min, respectively. The critical temperature of all the deposited films is higher than 9.1 K.

The results of the stress experiments are shown in fig. 8. At an Ar pressure of 2.0 Pa. zero stress can be achieved at a cathode voltage of −265 V. At an Ar pressure of 2.5 Pa, Nb films deposited at −265 V

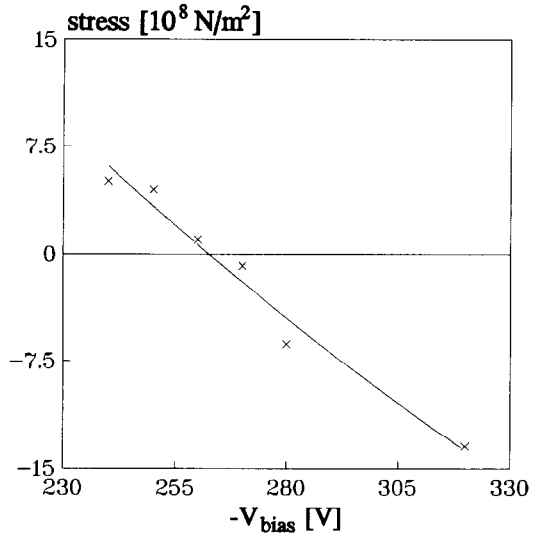

Fig. 8. Stress in Nb sputter deposited films as a function of the cathode voltage at an Ar sputter pressure of 2.0 Pa. The solid line is a guide to the eye.

showed a pronounced tensile stress. This is in contradiction with the experiments reported in ref. [21]. The dependence of the stress on the sputter conditions is probably different in differing sputtering systems. The "zero stress voltage" also changes with the thickness of the Nb target.

After structuring the oxidized top layer of the Si wafer, 150 nm (stress free) Nb and 5 nm of Al is deposited. The Al layer is thermally oxidized in the sputter chamber at room temperature in pure O_2. After oxidation, 4 nm Al is deposited followed by the deposition of 250 nm Nb (fig. 7(b)). This multilayer is structured by lift-off.

The thickness of the next layer of photo resist (thinned with AZ 1500) is 1.35 μm. After structuring, the resist is baked at 90°C. A higher post-baking temperature does not reduce the etch rate during the subsequent RIE process. This resist mask defines the junction areas as well as the contact areas with the base electrode. The second lithography step is followed by the selective Nb etching process (SNEP) in an RF SF_6 plasma. The Nb is etched at a DC self-bias voltage of −100 V, under the same conditions as described in section 2. The etch rates of SiO_2 and photo resist are 12 and 20 nm/min, respectively. During the SNEP, 250 nm of SiO_2 is etched away. After this step the SiO_2 surface is planarized with respect to the AlO_x barrier.

The remaining $Al,AlO_x/Al$ layer is etched away in a solution of photo resist developer (AZ 351) in H_2O with a volume ratio of 1:25 (AZ 351:H_2O) (fig. 7(c)). The reactive component in this developer is NaOH (4 wt.%). The Al etch rate is 2 nm/s. Nb is not etched by the developer. The etching time is 30 s, during which the photo resist is not affected. With shorter etching times the number of junctions which show leakage currents increases. The Al layers can also be removed by plasma etching in Ar, but with this technique redeposition of Al will occur, introducing metallic shorts over the junctions. Junctions in which the Al layers were removed by Ar etching often showed small leakage currents.

After the junctions are defined by SNEP, a self-aligned SiO_2 layer is deposited (fig. 7(d)). The SiO_2 film is grown by RF sputtering from a 4 inch target. The RF power on the target is 150 W inducing a self bias of −500 V. With the anode connected to ground, at first a thin layer (±20 nm) of SiO_x is sputtered at an Ar pressure of 2.5 Pa, to protect the photo resist. The sputtering is continued in an Ar/O_2 mixture with a flow ratio of $Ar:O_2$ of 10:1, at the same total pressure. Part of the SiO_2 layer is grown by SiO_2 bias sputtering with a bias power density of 0.06 W/cm^2 on the substrate. The deposition rate is 0.43 nm/min without bias and 0.40 nm/min with bias. The total SiO_2 thickness is 250 nm.

The final step (after an optional fabrication of Pd shunt resistors (fig. 7(e))) is the deposition of Nb contacts. This Nb film is structured by lift-off (fig. 7(f)).

4. *I–V* measurements

Low noise, battery powered electronics has been used to measure the *I–V* characteristics of the junctions. The input noise of the amplifiers is 5 nV/$\sqrt{}$Hz. The current is fed through a 1 kΩ resistor at room temperature in order to measure the bias current. The amplifiers have a bandwidth of 80 kHz and an input impedance of 10 MΩ.

Two junction series will be discussed: mb@10 and mb@11. The oxidation pressure during Al oxidation

was 10 mbar in series mb@10 and 1 mbar in series mb@11.

In fig. 9 the I–V curves of a 5×5 μm^2 junction of series mb@10 at 4.2 and 1.6 K are shown. The characteristics have been measured without suppression of the zero voltage current. The V_m value at 2 mV of this junction is 70 mV. (V_m is calculated from $V_m = I_{co}R_2$, where R_2 is the subgap resistance at 2 mV and I_{co} is the theoretical maximum zero-voltage current. I_{co} is calculated from the gap voltage V_g and the normal state resistance at 4 mV R_n: $I_{co} = \pi V_g/(4R_n)$.) During cooling to 1.6 K, V_m increases to 4.1 V. As far as we know, this is the highest value of V_m that has been reported for Nb/Al,AlO_x(/Al)/Nb junctions.

Series mb@10 also contains junctions of 3×3 and 2×2 μm^2 with V_m (4.2 K) values of 69 mV. The subgap current at 1.6 K of these junctions is of the order of the noise level of our measurement setup. Obviously, the AlO_x barrier in these junctions is very homogeneous.

As can be seen in fig. 9, the subgap current at 1.6 K increases at $V = V_{gap}/2$. This temperature-independent excess current can be explained by multiparticle tunneling, Josephson self-coupling or multiple Andreev reflections [24–27]. The excess currents determine the minimum subgap current at 2 mV that can be obtained by cooling. At 4.2 K this temperature independent tunneling current is only 1.8% of the total current at 2 mV.

In fig. 10 the I–V curves at 4.2 and 1.6 K of a 2×2 μm^2 junction of series mb@11 are shown. This junction has $V_m(4.2\text{ K}) = 69$ mV and $V_m(1.6\text{ K}) = 2.1$ V.

The highest $V_m(4.2\text{ K})$ value of a 1×1 μm^2 junction that has been obtained is 64 mV. The reproducibility of the area of these junctions, however, is bad. The fabrication of these small structures is limited by the optical lithography available in our laboratory.

Theoretical BCS I–V curves are shown in figs. 9 and 10 as well. At 4.2 K the subgap current can very well be described by the BCS theory. At 1.6 K the measured currents at 2 mV are about one order of magnitude higher than the values predicted by the BCS theory.

The I–V characteristics of 60 junctions of 4, 9, and 25 μm^2 of series mb@10 and mb@11 have been measured in total (30 junctions of each series). The V_m value of 43 junctions (72%) was larger than 60 mV. 51 Junctions (85%) showed a V_m larger than 50

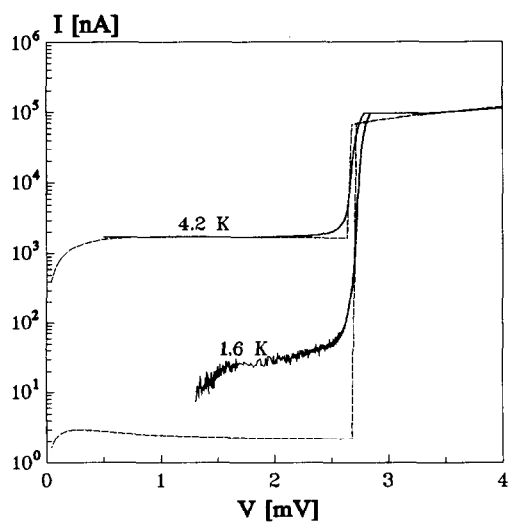

Fig. 9. Current–voltage characteristics of a 5×5 μm^2 junction of series mb@10 measured at 4.2 and at 1.6 K. The junction was current biased. The zero voltage current was not suppressed. The dashed lines are the theoretical BCS I–V curves at 4.2 and 1.6 K.

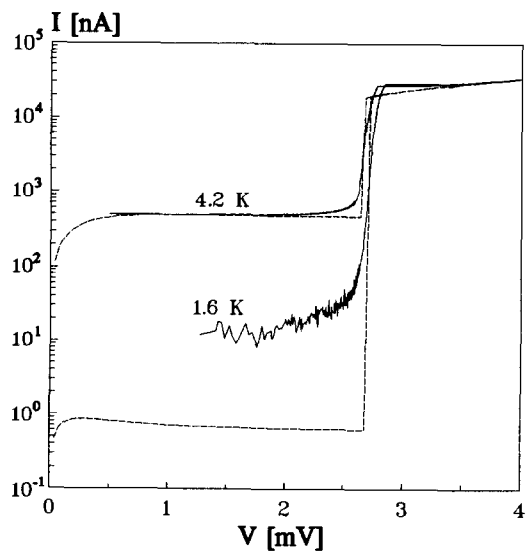

Fig. 10. Current–voltage characteristics of a 2×2 μm^2 junction of series mb@11 measured at two different temperatures. The junction was current biased. The zero voltage current was not suppressed. The theoretical BCS curves (dashed lines) are shown as well.

mV. No relation was found between the average quality of the junctions and the junction area.

As mentioned in section 3, junctions of 2×2 and 3×3 μm^2 with base Nb electrodes of 10×10, 15×15, 30×30, 50×50, and 100×100 μm^2 have been made. At 4.2 K the V_m value of all these junctions range from 64 to 66 mV in series mb@11. This confirms that the Nb electrodes of the junctions are free of stress.

The new fabrication process has obviously led to a significant improvement of the junction quality. In the fabrication process that was based on SNAP,the V_m value of 5×5 μm^2 junctions usually was about 50 mV. With the new process very high quality junctions with V_m values of 60–70 mV can be made in a reproducible way. The junction quality is the same for junctions of 25, 9 and 4 μm^2. It is expected that with e-beam lithography sub-micrometer junctions with comparable quality can be fabricated with this process.

5. Conclusions

A fabrication process has been developed to make very high quality, planar $Nb/Al,AlO_x/Al/Nb$ SNINS Josephson tunnel junctions with the help of selective niobium etching in SF_6. Junctions with areas ranging from 4 to 25 μm^2 have been made with V_m(4.2 K) values higher than 60 mV in more than 70% of the junctions. At 4.2 K the subgap current is almost completely determined by quasiparticle tunneling; only about 3% of the subgap current at 2 mV is due to temperature independent tunneling currents. At 1.6 K, the highest V_m value that has been measured is 4.1 V. This shows that the AlO_x barrier of the junctions is very homogeneous. It is expected that this fabrication process can be easily extended to sub-micrometer dimensions with the help of an appropriate lithography process.

Reactive ion etching of Nb in an RF SF_6 plasma has been studied in detail. At low RF power a high Nb etch rate (60 nm/min) and anisotropic etch profiles have been obtained. The Nb etch rate is dependent on the history of the reactor. Therefore, precleaning of the etching chamber is essential for reproducible results. Etching of Nb under the photo resist is prevented by a resistant layer that is formed during RIE on the sides of the Nb structure below the photo resist pattern. The etching process can be monitored very well by measuring the emission intensity of fluorine radicals at 703.7 nm. Thin Al films can be used as an etch stop after Nb etching if the self-bias voltage is 100 V or smaller.

Acknowledgement

These investigations in the program of the Foundation for Fundamental Research on Matter (FOM) have been supported (in part) by the Netherlands Technology Foundation (STW).

References

[1] M. Gurvitch, M.A. Washington and H.A. Huggins, Appl. Phys. Lett. 42 (1983) 472.
[2] E.C.G. Kirk, M.G. Blamire, R.E. Somekh, J.E. Evetts, D. van Vechten and N. Lovelet, IEEE Trans. Magn. 27 (1991) 3137.
[3] D.J. Adelerhof, E.P. Houwman, P.B.M. Fransen, D. Veldhuis, J. Flokstra and H. Rogalla, IEEE Trans. Magn. 27 (1991) 3153.
[4] M.B. Ketchen, D. Pearson, A.W. Kleinsasser, C.-K. Hu, M. Smyth, J. Logan, K. Stawiasz, E. Baran, M. Jaso, T. Ross, K. Petrillo, M. Manny, S. Basavaiah, S. Brodsky, S.B. Kaplan, W.J. Gallagher and M. Bhushan, Appl. Phys. Lett. 59 (1991) 2609.
[5] M. Bhushan and E.M. Macedo, Appl. Phys. Lett. 58 (1991) 1323.
[6] A.W. Lichtenberger, D.M. Lea, C. Li, F.L. Lloyd, M.J. Feldman, R.J. Mattauch, S.-K. Pan and A.R. Kerr, IEEE Trans. Magn. 27 (1991) 3168.
[7] V. Foglietti, W.J. Gallagher and R.H. Koch, IEEE Trans. Magn. Magn. 23 (1987) 1150.
[8] S. Kuriki, M. Matsuda and A. Matachi, J. Appl. Phys. 64 (1988) 239.
[9] B. Savo, F. C. Wellstood and J. Clarke, Appl. Phys. Lett 50 (1987) 1757.
[10] C.T. Rogers and R.A. Buhrman, Phys. Rev. Lett. 53 (1984) 1272.
[11] M. Kurakado, T. Takahashi and A. Matsumara, Appl. Phys. Lett. 57 (1990) 1933.
[12] D.J. Adelerhof, B. David, M.E. Bijlsma, J. Flokstra and H. Rogalla, Proc. 4th Int. Conf. SQUID'91, Berlin, Superconducting Devices and Their Applications, eds. H. Koch and H. Lübbig (Springer, Berlin, 1992) p. 203.
[13] R. Fromknecht, M Neuhaus and W. Jutzi, SQUID'85, eds. H.D. Hahlbohm and H. Lübbig (W. de Gruyter, Berlin-New York, 1985) p. 659.

[14] T.T. Foxe, B.D. Hunt, C. Rogers, A.W. Kleinsasser and R.A. Buhrman, J. Vac. Sci. Technol. 19 (1981) 1394.
[15] A.W. Lichtenberger, D.M. Lea and F.L. Lloyd, preprint Applied Superconductivity Conference, Chicago (1992).
[16] K.A. Blanks, A.E. Tabor and K. Becker, J. Chem. Phys. 86 (1987) 4871.
[17] D. Field, A.J. Hydes and D.F. Klemperer, Vacuum 34 (1984) 563.
[18] A.M. Casanovas, J. Casanovas, V. Dubroca, F. Lagarde and A. Belardi, J. Appl. Phys. 70 (1991) 1220.
[19] Gmelins Handbuch der anorganischen chemie, 8. auflage, Niob teil B1 (Verlag Chemie, GMBH, Weinheim/Bergstr., 1970).
[20] K. Kuroda and M. Yuda, J. Appl. Phys. 63 (1988) 2352.
[21] A.E. Hill and G.R. Hoffman, Brit. J. Appl. Phys. 18 (1967) 13.
[22] T. Imamura, T. Shiota and S. Hasuo, ISEC'91, ext. abstracts (1991) 29.
[23] T. Imamura, T. Shiota and S. Hasuo, IEEE Trans. Appl. Supercond. 2 (1992) 1.
[24] J.R. Schrieffer and J.W. Wilkins, Phys. Rev. Lett. 10 (1963) 17;
B.N. Taylor and E. Burstein, Phys. Rev. Lett. 10 (1963) 14.
[25] N.R. Werthamer, Phys. Rev. 147 (1966) 147.
[26] P. Mukhopadhyay, J. Phys. F 9 (1979) 903.
[27] T.M. Klapwijk, G.E. Blonder and M. Tinkham, Physica B 109–110 (1982) 1657.